CHIN. PHYS. LETT. Vol. 37, No. 9 (2020) 097201

Chalcogenide Perovskite $YScS_3$ as a Potential p-Type Transparent Conducting Material

Han Zhang(张涵)[1,2], Chen Ming(明辰)[2*], Ke Yang(杨科)[3,4], Hao Zeng(曾浩)[5], Shengbai Zhang(张绳百)[3], and Yi-Yang Sun(孙宜阳)[2*]

[1]*School of Materials Science and Engineering, Shandong University, Jinan 250061, China*
[2]*State Key Laboratory of High Performance Ceramics and Superfine Microstructure, Shanghai Institute of Ceramics, Chinese Academy of Sciences, Shanghai 201899, China*
[3]*Department of Physics, Applied Physics & Astronomy, Rensselaer Polytechnic Institute, Troy, New York 12180, USA*
[4]*School of Physics and Electronics, Hunan University, Changsha 410082, China*
[5]*Department of Physics, University at Buffalo, The State University of New York, Buffalo, New York 14260, USA*

(Received 26 August 2020; accepted 27 August 2020; published online 28 August 2020)

Transparent conducting materials (TCMs) have been widely used in optoelectronic applications such as touchscreens, flat panel displays and thin film solar cells. These applications of TCMs are currently dominated by n-type doped oxides. High-performance p-type TCMs are still lacking due to their low hole mobility or p-type doping bottleneck, which impedes efficient device design and novel applications such as transparent electronics. Here, based on first-principles calculations, we propose chalcogenide perovskite $YScS_3$ as a promising p-type TCM. According to our calculations, its optical absorption onset is above 3 eV, which allows transparency to visible light. Its hole conductivity effective mass is $0.48m_0$, which is among the smallest in p-type TCMs, suggesting enhanced hole mobility. It could be doped to p-type by group-II elements on cation sites, all of which yield shallow acceptors. Combining these properties, $YScS_3$ holds great promise to enhancing the performance of p-type TCMs toward their n-type counterparts.

PACS: 72.80.Cw, 71.20.Mq, 42.25.Bs, 61.72.uf DOI: 10.1088/0256-307X/37/9/097201

Introduction. Transparent conducting materials (TCMs) are transparent to visible light and, meanwhile, highly conductive to electrons. By combining the two seemingly incompatible properties, TCMs have found unique applications, e.g., in touchscreens, flat panel displays, and thin film solar cells. Currently, widely used TCMs are exclusively oxides, i.e., In_2O_3, SnO_2, and ZnO.[1–4] These transparent conducting oxides (TCOs) are all n-type doped. The p-type doping of these materials has been notoriously difficult. A main reason is that the valence bands derived from O $2p$ orbitals are too deep to allow shallow acceptors.[5,6] If the performance of p-type TCMs can be on par with their n-type counterparts, not only can the structure design of existing devices be more flexible, but also new transformative applications, such as transparent electronics, could be envisaged.[7–9] This driving force has motivated a vast amount of research developing p-type TCMs.[10–17]

Given the success of TCOs, oxides have been first explored for p-type TCMs with $CuAlO_2$ and NiO being representative examples.[9,18–20] For these oxides, the p-type doping problem can be solved because the Cu- and Ni-based compounds have relatively high valence band due to the interaction of the $3d$ electrons and O $2p$ valence band.[6] However, the localized O $2p$ orbitals usually result in rather large hole effective masses. As a result, the hole conductivity of oxides is usually on the order of several $S{\cdot}cm^{-1}$,[20] which is to be compared with $10^4\,S{\cdot}cm^{-1}$ typically achieved by n-type TCOs.[1] For this reason, non-oxide TCMs have been extensively explored.[7] Hole conductivity of two orders of magnitude higher than that of oxides has been achieved by chalcogenides and halides. Currently, the highest reported conductivity in polycrystalline p-type TCMs is $283\,S{\cdot}cm^{-1}$, achieved by CuI.[21,22] Similar high conductivity of $250\,S{\cdot}cm^{-1}$ has also been reported in $CuAlS_2$.[23] Given these encouraging works, the search for novel non-oxide high-performance p-type TCMs have been the subject of a number of recent studies.[15–17]

Chalcogenide perovskites recently emerge as novel functional materials. Due to the high structure stability, appropriate band gap and good optoelectronic

Y.-Y. Sun was supported by the National Natural Science Foundation of China (Grant No. 11774365). C. Ming was supported by the Natural Science Foundation of Shanghai, China (Grant No. 19ZR1421800) and the Science Foundation for Youth Scholar of State Key Laboratory of High Performance Ceramics and Superfine Microstructures (Grant No. SKL 201804). H. Zeng was supported by the U.S. NSF (Grant Nos. CBET-1510121 and CBET-1510948). K. Yang and S. Zhang were supported by the U.S. DOE (Grant No. DE-SC0002623).
*Corresponding author. Email: mingchen@mail.sic.ac.cn; yysun@mail.sic.ac.cn
© 2020 Chinese Physical Society and IOP Publishing Ltd

properties, some of these materials have been considered as promising candidates for light-absorbing and light-emitting applications.[24–31] In this Letter, we propose chalcogenide perovskite $YScS_3$ for light-transmitting application, as a new p-type TCM. $YScS_3$ has been experimentally synthesized half a century ago, but has not been considered as a functional material yet. Here, based on first-principles calculations, we found that (1) its optical absorption onset is above 3 eV allowing transparency to visible light; (2) it has a hole conductivity effective mass of $0.48m_0$, which is among the smallest in p-type TCMs; (3) it could be doped to p-type by group-II elements on cation sites, all of which yield shallow acceptors. These properties as the key indicators for an excellent TCM render the perovskite $YScS_3$ a promising candidate for p-type TCMs.

Computational Method. First-principles calculations in this work were mainly based on density functional theory (DFT). We carried out the calculations using the VASP program.[32] Projector augmented wave (PAW) potentials[33] were used to describe the interaction between ion cores and valence electrons. The wavefunctions were expanded by plane-wave basis sets. Hierarchical exchange-correlation functionals were used in our calculations for different purposes: (1) PBEsol functional[34] being computationally efficient was adopted in molecular dynamics (MD) simulations; (2) strongly constrained and appropriately normed (SCAN) functional[35] was used in calculations on atomic structures and thermodynamic stability of bulk and defects; (3) hybrid HSE functional[36] was used in calculations on band structures, optical absorption, and defect transition levels; (4) PBE functional was used to generate the starting wavefunctions for the G_0W_0 calculations, which produces the quasiparticle band gap.[37]

Planewave cutoff energy was taken to be 408 eV whenever cell volume is to be optimized, otherwise, it was taken to be 272 eV. An orthorhombic $2\times2\times2$ supercell of 160 atoms was used in the MD simulations. Another monoclinic 160-atom supercell, generated by a conversion matrix of (2 0 0; 0 1 −1; 0 2 2) was used in defect calculations to better separate the dopant atoms. Γ point was used in the supercell calculations to represent the Brillouin zone. In bulk calculations, the product of the number of k-points and the length of the lattice vector along each direction was greater than 40 Å. In the G_0W_0 calculations, 880 unoccupied bands, a Γ-centered $6\times4\times6$ k-point grid and 380 eV plane-wave cutoff energy were used.

The phonon spectra at 0 K was calculated using finite displacement method as implemented in the PHONOPY package.[38] A $2\times1\times2$ supercell was used in second-order force constant calculations. The k-point grids for the unit cell and supercell were consistent to ensure high accuracy in force constant calculations. The phonon spectra at elevated temperatures were obtained by the temperature-dependent effective potential (TDEP) method.[39] MD simulations with an NVT ensemble were performed at different temperatures. The simulations were run for 50 ps with a time step of 2 fs. The force constants were extracted from the simulations in the last 40 ps.

Results and Discussion. Experimentally, it is reported that $YScS_3$ has a crystal structure with $Pna2_1$ (No. 33) space group symmetry,[40] which is distorted from the perovskite structure with $Pnma$ (No. 62) space group by slightly displacing the Sc atom away from the octahedron center. The determination of space group, however, could be subject to uncertainty. For example, the space group of $CeScS_3$ was redetermined after the initial study[41] and reported to be $Pnma$.[42,43] In this work, we started from the experimental structure and carried out relaxations using PBEsol, SCAN, and HSE functionals. All methods ended up with the $Pnma$ symmetry.

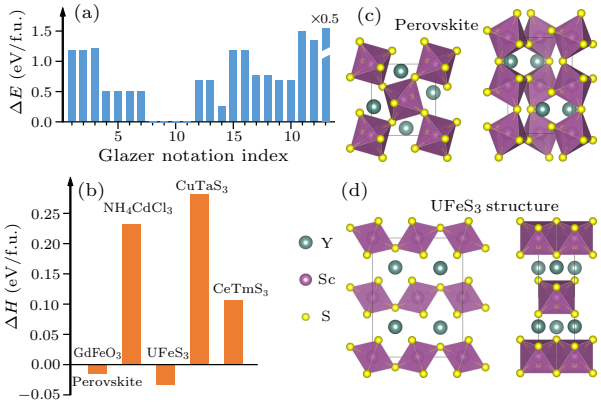

Fig. 1. (a) Relative energy of $YScS_3$ in 23 octahedron rotation patterns following Glazer's notation with respect to the lowest energy pattern. (b) Enthalpy of formation of $YScS_3$ in five different structures. (c) Atomic structure of $YScS_3$ in the $GdFeO_3$ (i.e., perovskite) structure in two different views. (d) Atomic structure of $YScS_3$ in the $UFeS_3$ (or post-perovskite) structure in two different views.

We also carried out a systematic determination of the particular octahedron rotation pattern in the perovskite structure by employing Glazer's notation,[44] which classified the octahedron rotation into 23 possibilities. In these calculations, we employed a supercell containing 8 octahedra (i.e., a $2\times2\times2$ supercell based on the non-distorted cubic perovskite unit cell) to accommodate the alternating octahedron rotations between nearest neighbors. PBEsol functional was used in these calculations. Figure 1(a) shows the calculated total energy with respect to the most stable rotation pattern. After relaxation, the patterns from 8 to 11 all yielded the $Pnma$ structure, which is the lowest energy configuration. Based on the results above, we

consider that $YScS_3$ is in the *Pnma* perovskite structure in this work.

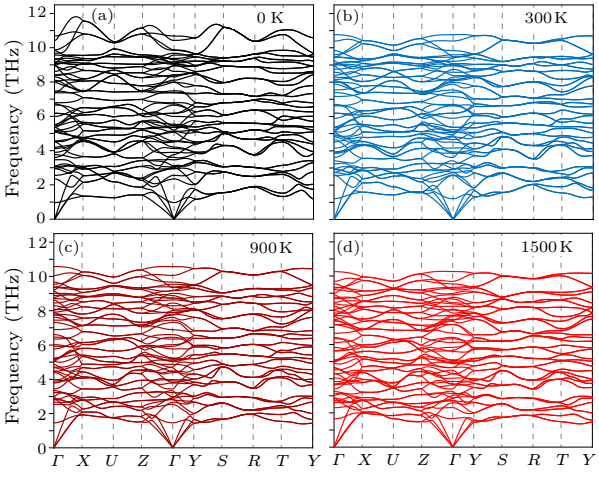

Fig. 2. The phonon spectra of $YScS_3$ in the perovskite structure at various temperatures. The TDEP method was used to extract the phonon spectra from MD simulations at corresponding temperatures.

We next compared the *Pnma* perovskite structure (or $GdFeO_3$ structure) with other possible structures that could be adopted by the ABS_3 compounds. Figure 1(b) shows the calculated enthalpy of formation of $YScS_3$ in different structures with respect to binary sulfides, Y_2S_3 and Sc_2S_3, which are in structures with space groups of *Pnma* and *Fddd* (No. 70), respectively. The SCAN functional was used to optimize the structure and calculate the total energies. We first considered the NH_4CdCl_3 structure, which is the structure of a number of ABS_3 compounds, such as $BaSnS_3$[45] and $SrZrS_3$.[46] Another structure with hexagonal lattice and space group $P6_3/mmc$ (No. 194), as adopted by $BaTiS_3$,[47] has rather high energy (about 2.6 eV higher than the perovskite structure) and is not shown in Fig. 1(b). The next important structure in Fig. 1(b) is the $UFeS_3$ structure,[48] which is also called post-perovskite structure in the literature.[49] According to our calculation, $YScS_3$ in this structure is slightly more stable than the perovskite structure. However, the energy difference is only 17 meV per formula unit (f.u.) of $YScS_3$. Given the fact that $YScS_3$ experimentally exists in the perovskite structure, this small energy difference is considered to be either the uncertainty in the calculation method or the possibility of another phase of $YScS_3$ to be discovered experimentally. The optimized lattice constants and atomic coordinates of this structure are given in the Supplementary Material. Another two considered structures are the $CuTaS_3$[50] and $CeTmS_3$[51] structures. The latter structure is also adopted by $LaYS_3$, which was recently proposed for photocatalytic applications.[52] Our results show that these two structures are not competitive to the perovskite structure. Figures 1(c) and 1(d) show the atomic structures of $YScS_3$ in the perovskite and $UFeS_3$ structures, respectively, which will be discussed below in more details.

To further check the stability of $YScS_3$ in the perovskite structure at high temperatures, we carried out MD simulations and extracted phonon spectra from the MD trajectories, as shown in Fig. 2. No imaginary modes are observed in the spectra from 0 K up to 1500 K, suggesting its kinetic stability. When the temperature is increased, the high-frequency optical modes become softened, i.e., their frequencies decrease. In contrast, the low-frequency optical modes, especially the lowest mode at the Γ point, are hardened. Usually, the soft modes close to zero indicate the direction of phase change or kinetic instability. The hardening of soft modes suggests that increased temperature helps stabilize the perovskite structure.

After evaluating the stability of $YScS_3$ in the perovskite structure, we next study its optoelectronic properties. Figure 3(a) shows the band structure of perovskite $YScS_3$, which has an indirect gap with the valence band maximum (VBM) at the Γ point and the conduction band minimum (CBM) at the Y point. The indirect gap from HSE calculation is 2.79 eV, while the direct gap at the Γ point is 2.98 eV. Figure 3(b) shows the partial charge density plots for the VBM state at the Γ point (bottom panel) and the CBM state at the Y point (middle panel). Also shown is the lowest unoccupied state at the Γ point (top panel), referred to as CBM-Γ state. It can be seen that the VBM state is predominantly composed of S $3p$ orbitals, while the CBM-Γ state is predominantly composed of Sc $3d$ orbitals. Not unexpected, the CBM state is a hybridized state between the Y $4d$ and Sc $3d$ orbitals. The lower energy of the CBM state than the CBM-Γ state is possibly a result of the stronger coupling between the Y $4d$ and Sc $3d$ orbitals at the Y point. To further confirm the predicted band gap, we used the quasi-particle G_0W_0 calculation. The indirect gap from Γ to Y is found to increase to 3.16 eV and the direct gap at the Γ point is increased to 3.46 eV. It is expected that the actual band gap of perovskite $YScS_3$ is located between the HSE and G_0W_0 results.

Figure 3(c) shows the band structure of $YScS_3$ in the $UFeS_3$ structure. Here, the direct gap at the Γ point is 2.12 eV and the indirect gap between the VBM at the Γ point and the CBM at the Y point is 1.30 eV. Both values are significantly smaller than that in the perovskite structure. In the $UFeS_3$ structure, the VBM state is still contributed by S $3p$ orbitals. Different from the case in the perovskite structure, however, the CBM and CBM-Γ states are contributed by Y $4d$ and Sc $3d$ orbitals exclusively. It is worth noting that the isosurface values in the plots in Figs. 3(b)

and 3(d) depend on the states. For the CBM states, the value is 0.005 electron/Å^3, while for the VBM and CBM-Γ states, the value is set to be 50 times smaller, suggesting that the CBM states are much more delocalized.

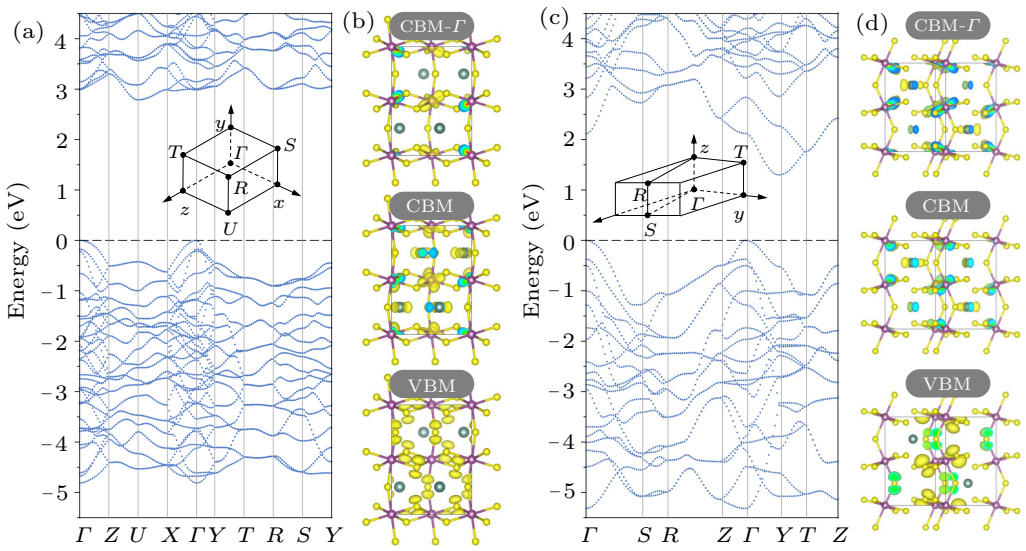

Fig. 3. (a) Band structure of $YScS_3$ in the perovskite structure obtained using HSE calculation. Inset shows the Brillouin zone and the high-symmetry k points. (b) Partial charge density plots of VBM and CBM states, as well as the CBM state at the Γ point. (c) and (d) are similar to (a) and (b), but for $YScS_3$ in the $UFeS_3$ structure.

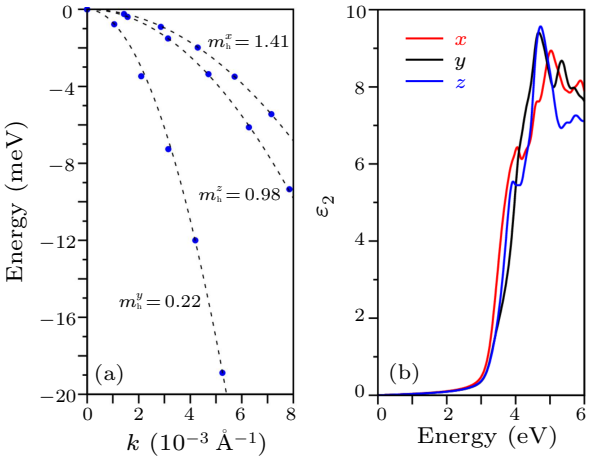

Fig. 4. (a) Parabolic fitting of the top valence band of perovskite $YScS_3$ along Γ–X, Γ–Y, and Γ–Z directions to obtain the effective masses of holes along the three directions. The data points were obtained using HSE + SOC calculation. The unit of effective masses is m_0, the mass of an electron. (b) Imaginary part of dielectric constant (ε_2) of perovskite $YScS_3$ along the three directions obtained using HSE calculation.

The figure of merit of a TCM can be expressed as the ratio of electrical conductivity to optical absorption coefficient for visible light. As a p-type TCM, the electrical conductivity is intrinsically determined by the effective mass of holes and, in addition, by a variety of carrier scattering mechanisms. We calculated the hole effective masses by a parabolic fitting to the top valence band using the HSE functional plus SOC effect (HSE + SOC). The results are shown in Fig. 4(a). The top valence band near the Γ point shows anisotropy. The Γ–Y direction exhibits more prominent band dispersion with an effective mass of $0.22m_0$. The Γ–X and Γ–Z directions have an effective mass of $1.41m_0$ and $0.98m_0$, respectively. The conductivity effective mass of holes according to[53]

$$m_c = 3\left(\frac{1}{m_h^1} + \frac{1}{m_h^2} + \frac{1}{m_h^3}\right)^{-1} \quad (1)$$

is calculated to be $0.48m_0$, which is an attractive value for p-type materials. As a comparison, we calculated the m_c of holes for $CuAlS_2$, which has been demonstrated to exhibit the highest conductivity (250 S·cm^{-1}) among chalcogenide p-type TCMs. $CuAlS_2$ has a tetragonal structure. Our HSE + SOC calculation yielded $m_h^x = m_h^y = 1.14m_0$ and $m_h^z = 0.40m_0$, giving rise to $m_c = 0.71m_0$. Currently, the highest conductivity of polycrystalline p-type TCMs (283 S·cm^{-1}) is held by the halide CuI, which is in zinc-blende structure. According to our HSE + SOC calculation, its hole effective masses along the Γ–L, Γ–X, and Γ–K directions are $1.72m_0$, $0.60m_0$, and $1.24m_0$, respectively, giving rise to $m_c = 0.98m_0$. A longer list of effective masses of p-type TCMs as collected from a computational electronic transport database[54] is given in the Supplementary Material. The comparison suggests that perovskite $YScS_3$ having the smallest conductivity effective mass could im-

prove the conductivity of p-type TCMs toward their n-type counterparts.

The optical absorption coefficient is determined by the imaginary part of the dielectric constant (ε_2). For TCMs, it is required that the absorption onset is above 3 eV so that the visible light can be efficiently transmitted. Figure 4(b) shows the calculated ε_2 of perovskite $YScS_3$. The anisotropy here is weaker than that for effective masses as shown in Fig. 4(a). The three diagonal elements of ε_2 (i.e., ε_2^{xx}, ε_2^{yy}, and ε_2^{zz}) all exhibit weak absorption below 3 eV and sharp increase above that, ensuring perovskite $YScS_3$ to be a promising TCM. We also calculated the ε_2 of $YScS_3$ in the $UFeS_3$ structure, as shown in the Supplementary Material. Even though the indirect gap of $YScS_3$ in this structure is only 1.3 eV, its optical absorption onset is around 2.3 eV and the sharp increase occurs above 3 eV. It is expected that this phase will absorb a small portion of visible light in the green to violet region.

The conductivity is also determined by the carrier concentration, which in turn depends on the doping efficiency. For wide gap semiconductors like TCMs, the doping bottleneck is often a challenging issue. The widely used TCO materials all suffer from the difficulty of p-type doping.[5,6] Here, for $YScS_3$ we considered group-II element (Mg, Ca, Sr, Ba, and Zn) doping on the Y and Sc sites. The defect transition level between two charge states q and q' was determined by

$$\epsilon\,(q/q') = \left(E_{\rm D}^{q} - E_{\rm D}^{q'}\right)/\left(q' - q\right) - E_{\rm VBM}, \qquad (2)$$

where $E_{\rm D}^{q}$ and $E_{\rm D}^{q'}$ are the total energies of the defect supercell in the q and q' charge states and $E_{\rm VBM}$ is the Kohn–Sham eigenvalue of the VBM state. Our results obtained using the SCAN functional show that group-II elements on both Y and Sc sites are all shallow acceptors with $\epsilon\,(0/-)$ smaller than 0.01 eV above the VBM. The formation energies from the SCAN functional, as listed in the Supplementary Material, suggest that Mg prefers to be on the Sc sites, Ca, Sr, and Ba prefer to be on the Y sites, while Zn shows similar formation energy on the two sites. Sr-on-Y (Sr_Y) doping is energetically the most favored.

We further calculated the formation energy of Sr_Y and S vacancy (V_S) as a function of Fermi level (E_F) using the HSE functional. The p-type $YScS_3$ requires to be prepared under S-rich conditions to avoid the compensation due to intrinsic donor defects, especially, V_S. Figure 5 is obtained using the S-rich condition. It can be seen that under the S-rich condition, the V_S defect has rather high formation energy. According to Fig. 5, the lowest formation energy of V_S is 1.03 eV at the VBM, while the formation energy of Sr_Y is only slightly higher than V_S by 0.15 eV, which results in the pinned E_F at 0.05 eV above the VBM, suggesting a good p-type semiconductor by Sr doping. It is noted that V_S is a deep donor according to our HSE calculation. The inset of Fig. 5 shows the partial charge density of V_S corresponding to the Kohn–Sham state in the band gap, which is rather localized. For the charged localized defects, it is necessary to consider the interaction between the periodic images of the localized charge. For this purpose, we considered the Madelung correction, which could overestimate the image-charge interaction, but the error is usually small for image distance above 15 Å.[55] The correction for +2 and +1 states of V_S is 0.85 and 0.21 eV, respectively, using dielectric constant of 6.37 obtained from the optical absorption calculation above.

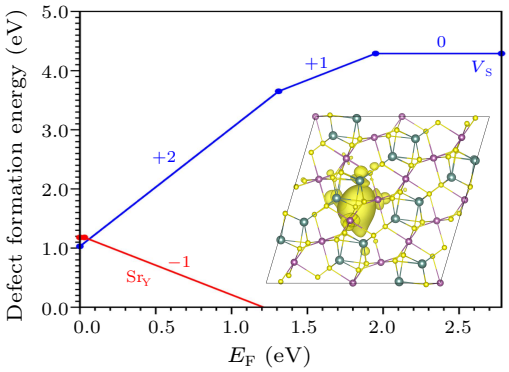

Fig. 5. Formation energy of Sr-on-Y (Sr_Y) p-type dopant and the intrinsic S vacancy (V_S) defect as a function of Fermi level (E_F), which is measured between the VBM and CBM calculated by HSE functional from the 160-atom supercell. The dots mark the transition energy between two charge states. The inset shows the partial charge density of the V_S defect state.

Conclusions. We propose that $YScS_3$ in the perovskite structure could be an excellent p-type TCM. To support this proposal, we carried out first-principles calculations on four aspects of the properties of $YScS_3$: stability, transparency, mobility, and doping. (1) Even though the perovskite is the only experimentally reported phase, there might exist a competing phase in the $UFeS_3$ structure, which is worth attention in future experiments. According to our calculated phonon spectra up to 1500 K, no sign of kinetic instability was observed in the perovskite $YScS_3$. (2) The optical absorption onset is predicted to be about 3 eV by hybrid HSE functional. G_0W_0 calculation suggests even higher onset by about 0.5 eV, ensuring full transmission of visible light. (3) The calculated conductivity effective mass of holes is $0.48m_0$, which is among the smallest in materials with the optical absorption onset above 3 eV. (4) The p-type doping could be achieved by group-II elements on the cation sites, all of which could produce shallow acceptors. With the predicted properties, it is expected that the performance of p-type TCMs could be improved over the

current state of the art towards that of n-type TCMs.

References

[1] Ellmer K 2012 *Nat. Photon.* **6** 809
[2] Morales-Masis M, De Wolf S, Woods-Robinson R, Ager J W and Ballif C 2017 *Adv. Electron. Mater.* **3** 1600529
[3] Liu H, Avrutin V, Izyumskaya N, Özgür Ü and Morkoç H 2010 *Superlattices Microstruct.* **48** 458
[4] Beyer W, Hüpkes J and Stiebig H 2007 *Thin Solid Films* **516** 147
[5] Zhang S B 2002 *J. Phys.: Condens. Matter* **14** R881
[6] Wei S H 2004 *Comput. Mater. Sci.* **30** 337
[7] Woods-Robinson R, Han Y, Zhang H, Ablekim T, Khan I, Persson K A and Zakutayev A 2020 *Chem. Rev.* **120** 4007
[8] Brunin G, Ricci F, Ha V A, Rignanese G M and Hautier G 2019 *npj Comput. Mater.* **5** 63
[9] Zhang K H L, Xi K, Blamire M G and Egdell R G 2016 *J. Phys.: Condens. Matter* **28** 383002
[10] Hautier G, Miglio A, Ceder G, Rignanese G M and Gonze X 2013 *Nat. Commun.* **4** 2292
[11] Bhatia A, Hautier G, Nilgianskul T, Miglio A, Sun J, Kim H J, Kim K H, Chen S, Rignanese G M, Gonze X and Suntivich J 2016 *Chem. Mater.* **28** 30
[12] Williamson B A, Buckeridge J, Brown J, Ansbro S, Palgrave R G and Scanlon D O 2016 *Chemistry of Materials* acs.chemmater.6b03306
[13] Woods-Robinson R, Broberg D, Faghaninia A, Jain A, Dwaraknath S S and Persson K A 2018 *Chem. Mater.* **30** 8375
[14] Youn Y, Lee M, Kim D, Jeong J K, Kang Y and Han S 2019 *Chem. Mater.* **31** 5475
[15] Varley J B, Miglio A, Ha V A, van Setten M J, Rignanese G M and Hautier G 2017 *Chem. Mater.* **29** 2568
[16] Wei L, Xu X, Gurudayal, Bullock J and Ager J W 2019 *Chem. Mater.* **31** 7340
[17] Kormath Madam Raghupathy R, Kühne T D, Felser C and Mirhosseini H 2018 *J. Mater. Chem. C* **6** 541
[18] Kawazoe H, Yasukawa M, Hyodo H, Kurita M, Yanagi H and Hosono H 1997 *Nature* **389** 939
[19] Sato H, Minami T, Takata S and Yamada T 1993 *Thin Solid Films* **236** 27
[20] Wang Z, Nayak P K, Caraveo-Frescas J A and Alshareef H N 2016 *Adv. Mater.* **28** 3831
[21] Yang C, Knei M, Lorenz M and Grundmann M 2016 *Proc. Natl. Acad. Sci. USA* **113** 12929
[22] Yamada N, Ino R and Ninomiya Y 2016 *Chem. Mater.* **28** 4971
[23] Huang F Q, Liu M L and Yang C 2011 *Sol. Energy Mater. Sol. Cells* **95** 2924
[24] Sun Y Y, Agiorgousis M L, Zhang P and Zhang S 2015 *Nano Lett.* **15** 581
[25] Perera S, Hui H, Zhao C, Xue H, Sun F, Deng C, Gross N, Milleville C, Xu X, Watson D F, Weinstein B, Sun Y Y, Zhang S and Zeng H 2016 *Nano Energy* **22** 129
[26] Gross N, Sun Y Y, Perera S, Hui H, Wei X, Zhang S, Zeng H and Weinstein B A 2017 *Phys. Rev. Appl.* **8** 044014
[27] Niu S, Milam-Guerrero J, Zhou Y, Ye K, Zhao B, Melot B C and Ravichandran J 2018 *J. Mater. Res.* **33** 4135
[28] Wei X, Hui H, Zhao C, Deng C, Han M, Yu Z, Sheng A, Roy P, Chen A, Lin J, Watson D F, Sun Y Y, Thomay T, Yang S, Jia Q, Zhang S and Zeng H 2020 *Nano Energy* **68** 104317
[29] Niu S, Huyan H, Liu Y, Yeung M, Ye K, Blankemeier L, Orvis T, Sarkar D, Singh D J, Kapadia R and Ravichandran J 2017 *Adv. Mater.* **29** 1604733
[30] Meng W, Saparov B, Hong F, Wang J, Mitzi D B and Yan Y 2016 *Chem. Mater.* **28** 821
[31] Hanzawa K, Iimura S, Hiramatsu H and Hosono H 2019 *J. Am. Chem. Soc.* **141** 5343
[32] Kresse G and Furthmüller J 1996 *Comput. Mater. Sci.* **6** 15
[33] Kresse G and Joubert D 1999 *Phys. Rev. B* **59** 1758
[34] Perdew J P, Ruzsinszky A, Csonka G I, Vydrov O A, Scuseria G E, Constantin L A, Zhou X and Burke K 2008 *Phys. Rev. Lett.* **100** 136406
[35] Sun J, Ruzsinszky A and Perdew J P 2015 *Phys. Rev. Lett.* **115** 036402
[36] Heyd J, Scuseria G E and Ernzerhof M 2003 *J. Chem. Phys.* **118** 8207
[37] Hybertsen M S and Louie S G 1986 *Phys. Rev. B* **34** 5390
[38] Togo A and Tanaka I 2015 *Scr. Mater.* **108** 1
[39] Hellman O, Abrikosov I A and Simak S I 2011 *Phys. Rev. B* **84** 180301
[40] Rodier N and Laruelle P 1970 *C. R. Acad. Sc. (Paris)* **C270** 2127
[41] Rodier N, Laruelle P and Flahaut J 1969 *C. R. Acad. Sc. (Paris)* **C269** 1391
[42] IJdo D 1980 *Acta Crystallogr. Sect. B* **36** 2403
[43] Range K J, Gietl A and Klement U 1993 *Z. Kristallogr.* **207** 147
[44] Glazer A 1972 *Acta Crystallogr. Sect. B* **28** 3384
[45] Yamaoka S and Okai B 1970 *Mater. Res. Bull.* **5** 789
[46] Lee C S, Kleinke K M and Kleinke H 2005 *Solid State Sci.* **7** 1049
[47] Hahn H and Mutschke U 1957 *Z. Anorg. Allg. Chem.* **288** 269
[48] Noel H and Padiou J 1976 *Acta Crystallogr. Sect. B* **32** 1593
[49] Murakami M, Hirose K, Kawamura K, Sata N and Ohishi Y 2004 *Science* **304** 855
[50] Crevecoeur C and Romers C 1964 *Proc. Koninklijke Nederlandse Acad. Van Wetenschappen* **67** 289
[51] Rodier N 1973 *Bull. La Societe Francaise Mineralogie Cristallographie* **96** 350
[52] Kuhar K, Crovetto A, Pandey M, Thygesen K S, Seger B, Vesborg P C K, Hansen O, Chorkendorff I and Jacobsen K W 2017 *Energy & Environ. Sci.* **10** 2579
[53] Sze S M 1969 *Physics of Semiconductor Devices* (New Jersey: Wiley)
[54] Ricci F, Chen W, Aydemir U, Snyder G J, Rignanese G M, Jain A and Hautier G 2017 *Sci. Data* **4** 170085
[55] Freysoldt C, Neugebauer J and van de Walle C G 2009 *Phys. Rev. Lett.* **102** 016402

Supplementary Material: Chalcogenide Perovskite $YScS_3$ as a potential p-Type Transparent Conducting Material

Han Zhang(张涵)[1,2], Chen Ming(明辰)[2*] , Ke Yang(杨科)[3,4], Hao Zeng(曾浩)[5], Shengbai Zhang(张绳百)[3], and Yi-Yang Sun(孙宜阳)[2*]

[1]School of Materials Science and Engineering, Shandong University, Jinan 250061, China

[2]State Key Laboratory of High Performance Ceramics and Superfine Microstructure, Shanghai Institute of Ceramics, Chinese Academy of Sciences, Shanghai 201899, China

[3]Department of Physics, Applied Physics & Astronomy, Rensselaer Polytechnic Institute, Troy, New York 12180, USA

[4]School of Physics and Electronics, Hunan University, Changsha, 410082, China

[5]Department of Physics, University at Buffalo, The State University of New York, Buffalo, New York 14260, USA

[*] **Corresponding authors. Email:** mingchen@mail.sic.ac.cn and yysun@mail.sic.ac.cn

The CIF file for the optimized structure of $YScS_3$ in perovskite structure

```
data_YScS3_in_perovskite_structure

_cell_length_a    6.9991
_cell_length_b    9.5258
_cell_length_c    6.3716
_cell_angle_alpha 90.
_cell_angle_beta  90.
_cell_angle_gamma 90.

_symmetry_space_group_name_H-M "P 21/n 21/m 21/a"
_symmetry_Int_Tables_number 62
_space_group.reference_setting '062:-P 2ac 2n'
_space_group.transform_Pp_abc a,b,c;0,0,0

loop_
_space_group_symop_id
_space_group_symop_operation_xyz
1 x,y,z
2 x+1/2,-y+1/2,-z+1/2
3 -x,y+1/2,-z
4 -x+1/2,-y,z+1/2
5 -x,-y,-z
6 -x+1/2,y+1/2,z+1/2
7 x,-y+1/2,z
8 x+1/2,y,-z+1/2

loop_
_atom_site_label
_atom_site_type_symbol
_atom_site_symmetry_multiplicity
_atom_site_Wyckoff_label
_atom_site_fract_x
_atom_site_fract_y
_atom_site_fract_z
_atom_site_occupancy
Y1  Y    4 c 0.40087 0.25000 0.04004 1.00000
Sc1 Sc   4 a 0.00000 0.00000 0.00000 1.00000
S1  S    4 c 0.04892 0.25000 0.85653 1.00000
S2  S    8 d 0.68506 0.42882 0.17658 1.00000
```

The CIF file for optimized structure of $YScS_3$ in $UFeS_3$ structure

```
data_YScS3_in_UFeS3_structure

_cell_length_a    3.7176
_cell_length_b   12.0855
_cell_length_c    9.1832
_cell_angle_alpha 90.
_cell_angle_beta  90.
_cell_angle_gamma 90.

_symmetry_space_group_name_H-M "C 2/m 2/c 21/m"
_symmetry_Int_Tables_number 63
_space_group.reference_setting '063:-C 2c 2'
_space_group.transform_Pp_abc a,b,c;0,0,0

loop_
_space_group_symop_id
_space_group_symop_operation_xyz
1 x,y,z
2 x,-y,-z
3 -x,y,-z+1/2
4 -x,-y,z+1/2
5 -x,-y,-z
6 -x,y,z
7 x,-y,z+1/2
8 x,y,-z+1/2
9 x+1/2,y+1/2,z
10 x+1/2,-y+1/2,-z
11 -x+1/2,y+1/2,-z+1/2
12 -x+1/2,-y+1/2,z+1/2
13 -x+1/2,-y+1/2,-z
14 -x+1/2,y+1/2,z
15 x+1/2,-y+1/2,z+1/2
16 x+1/2,y+1/2,-z+1/2

loop_
_atom_site_label
_atom_site_type_symbol
_atom_site_symmetry_multiplicity
_atom_site_Wyckoff_label
_atom_site_fract_x
_atom_site_fract_y
_atom_site_fract_z
_atom_site_occupancy
Y1  Y    4 c 0.00000 0.25275  0.25000 1.00000
Sc1 Sc   4 a 0.00000 0.00000  0.00000 1.00000
S1  S    4 c 0.00000 -0.08586 0.25000 1.00000
S2  S    8 f 0.00000 0.35849  0.56369 1.00000
```

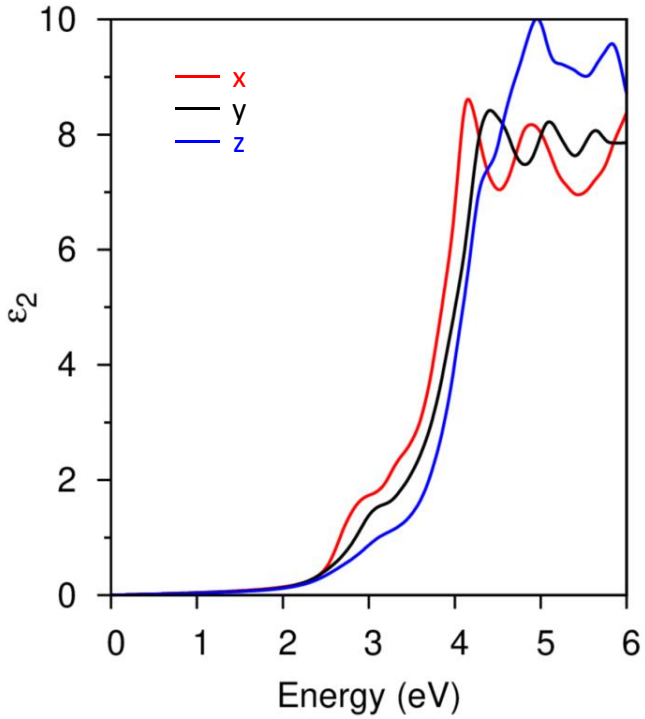

Figure S1. Imaginary part of dielectric constant (ε_2) of $YScS_3$ in the $UFeS_3$ structure.

Table S1. The hole effective mass of potential p-type transparent conducting materials. The unit is m_0. The values of m_h^1, m_h^2 and m_h^3 were collected from a computational electronic transport database,[1] which was generated using PBE functional without considering spin-orbit coupling (SOC) effect. The conductivity effective mass m_c was calculated according to the formula shown in the main text. It can be seen that none of these materials exhibit m_c smaller than 0.5 m_0.

	m_h^1	m_h^2	m_h^3	m_c
AlN	0.43	3.58	3.58	1.04
GaN	1.56	1.56	1.85	1.65
ZnO	1.85	1.85	2.96	2.11
ZnS	1.07	1.07	1.61	1.20
In_2O_3	6.05	6.05	6.05	6.05
SnO_2	1.47	1.47	2.11	1.64
$CuAlO_2$	1.92	1.92	5.22	2.43
$CuAlS_2$	1.02	1.76	1.76	1.42
$CuGaO_2$	2.46	2.46	5.00	2.96
CuI	0.86	0.86	0.86	0.86
BaCuSeF	0.69	0.69	253	1.03
BaCuTeF	0.52	0.52	137	0.78
Al_2Se_3	0.64	0.69	308	1.00
MgS	0.98	0.98	0.98	0.98
MgSe	1.24	1.24	1.24	1.24
MgTe	1.31	1.71	1.71	1.55

[1] F. Ricci, W. Chen, U. Aydemir, G. J. Snyder, G.-M. Rignanese, A. Jain, and G. Hautier, Scientific Data **4,** 170085 (2017).

Table S2. Calculated formation energy of p-type dopants at Y and Sc sites in neutral charge state using the SCAN functional. The unit is eV.

	Mg	Ca	Sr	Ba	Zn
On Y site	1.11	0.78	0.66	0.87	1.35
On Sc site	0.73	1.37	2.06	3.19	1.34